Efficient Dispersion of Organic Fluorophores by Size Matching with a Difunctionalized Spacer Interleaved into Layered Double Hydroxide

Guillaume Zerbib, Damien Boyer, Geneviève Chadeyron, François Réveret, Fabrice Leroux

Efficient Dispersion of Organic Fluorophores by Size Matching with a Di-Functionalized Spacer Interleaved into Layered Double Hydroxide

Guillaume Zerbib, Damien Boyer[*]*, Geneviève Chadeyron, François Réveret, and Fabrice Leroux*

Université Clermont Auvergne, CNRS, Clermont Auvergne INP, ICCF, F-63000 Clermont-Ferrand, France

Key words: Layered Double Hydroxide, Size Matching Interlayer Space (SMIS), Sulforhodamine B, Luminescent composite, Rare-earth-free phosphor, Luminescence decay, Silicone films

Abstract

Strongly luminescent when diluted in aqueous solution, Sulforhodamine B (SRB) is an organic dye suffering from aggregation caused quenching (ACQ) in its solid state. Its co-intercalation in very small quantities (0.12 mol%) in a layered double hydroxide (LDH) matrix with phenylenedipropionate (PPA) anions, a di-functionalized spacer matching its size, is found to be highly effective, with more than 99% of the SRB molecules uptaken. The resulting hybrid material enables luminescence with an absolute quantum yield ($PLQY_{abs}$) reaching 39% under UV excitation and even reaching 60% at its maximum. The dispersion of the LDH dye powder in

silicone results in homogeneous composite films with loading as high as 40 wt.% useable as masterbatch. The optical properties are found to remain after thermal treatment up to 120°C with a decrease in $PLQY_{abs}$ of 5% only, making it a good candidate for the development of rare-earth-free phosphors.

1. INTRODUCTION

Luminescent materials are in high demand in various fields, such as the development of display or lighting devices. Indeed, associated with a blue or UV chip they allow a coloured or white-light emitting diode (WLED) to be obtained [1–3]. The development and use of luminescent compounds containing rare-earth (RE) elements (europium, cerium, yttrium…) is currently predominant [2–7]. However, economic and environmental issues resulting from the exploitation of these RE elements [8–11] have made it a matter of concern for the European Union [12], thus encouraging the development of phosphors using other elements [2,13–15]. To employ an organic luminescent dye such as Sulforhodamine B (SRB) is a good alternative. This molecule of the Xanthene family, mostly studied in aqueous solution, is mainly used in anticancer drug development [16,17], watercourse mapping [18,19] or even offered to the general public to colour tattoos [20,21]. Its availability, low price, non-toxicity [22] and above all its strong red-orange emission (590 nm under green excitation in aqueous diluted solution) make it a molecule of choice for the development of RE-free phosphors. However, like a large number of organic dyes, SRB undergoes aggregation-caused quenching (ACQ) in its solid state [23]. Such a luminescent dye can be hosted in a restricted geometry, such as the voids of 2D interlayered or 3D mesoporous materials. Indeed, the immobilization of active species in structured matrices enables a dispersion of the molecules similar to that obtained in solutions [24]. Some recent works concerning the encapsulation of luminescent dyes in Metal-Organic Frameworks (MOFs) have

brought to light interesting optical properties [25–27]. Layered materials, due to their ability to organize and immobilize guest molecules such as metal phosphates, graphene oxide or perovskites, have been and still are being widely studied [28]. The final optical properties may vary depending on the dispersive medium used. For instance, Lamouche and Lavallard showed that the dielectric permittivity of the surrounding medium has an influence on the luminescent properties of dye molecules [29]. One of these layered structures is Layered Double Hydroxide (LDH) and is used as a host-guest material in various applications such as catalysis [30–32], medicine [33], adsorption [34] or electrochemistry [35,36]. This anionic clay, of the same structure as natural hydrotalcite (rhombohedral symmetry), can be described from the brucite $Mg(OH)_2$ structure which consists of the edge-sharing octahedral coordination of divalent metallic cations M^{2+} by hydroxyl groups to form anisotropic wide electroneutral layers. The LDH structure is obtained by replacing part of the M^{2+} cations by trivalent M^{3+} cations, resulting in an excess of positive charge in the layers [37]. Counterions such as carbonates, nitrates or anions of interest are interlayered in order to balance this positive charge excess and ensure electroneutrality. Some water molecules are also present between the LDH layers. Thus, the general formula of LDH can be written $[M^{2+}_{1-x}M^{3+}_{x}(OH)_2][A^{n-}]_{x/n}.mH_2O$, where M^{2+} is the divalent cation (Ca^{2+}, Zn^{2+}, Fe^{2+}, Mg^{2+}…), M^{3+} is the trivalent cation (Al^{3+}, Fe^{3+}, Cr^{3+}, Mn^{3+}…), A^{n-} is the interlayered counterion and m is the number of water molecules present between and at the surface of the LDH layers. Various studies have been carried out in the lighting field and have consisted in hosting phosphors in LDH in order to exploit their luminescence properties, such as rare-earth elements [38–40] or quantum dots [41–43]. Some organic dyes have been interleaved in a LDH structure, such as fluorescein [44,45], perylenes [46–48] or rhodamines [24,49]. Two works refer to the hosting of SRB in LDH, first by Yan et *al.* in 2008 [50] and more recently by us and co-workers.[15]. In these works,

the LDH matrices have shown their important role as solid solvents allowing sufficient dispersion and spacing of the SRB molecules between layers to avoid non-radiative energy transfers from aggregates and prevent luminescence quenching. Thermal and photonic stability is also provided by the LDH matrix to the organic dyes, which are known to be generally unstable over time. However, the correct formulation of the LDH-Phosphor composite is crucial to obtain a robust luminescent material. Indeed, the position and the environment of the interleaved dye can be more or less favourable to the phenomenon of luminescence quenching as observed by Bauer et *al.*, who obtained the total extinction of perylene bisimidetetrasulfonate after its intercalation in LDH [48]. In this search for the ideal formulation, it is sometimes necessary to add some surfactant molecules co-intercalated with the dye between the LDH layers. These molecules, called spacers, bind to the LDH layers in the same way the dye does, participate in the charge balance and must therefore be anionic. Their role is to 1) increase and adjust the basal spacing to enable a good diffusion of the dye within the LDH matrix and allow size matching between the interlayer space (SMIS) [41] and the guest molecules, 2) disperse and maintain them at a sufficient distance from each other to avoid aggregation and 3) offer compatibility for dispersion in polymers by providing an organophilic environment at the surfaces of the external LDH layers. Indeed, various works on spacers have been carried out to study their influence on final properties, such as those of Carrasco et *al.*, who showed that certain spacer sizes favour the oxygen evolution reaction [30]. Grover et *al.* demonstrated the importance of using an interleaved surfactant to separate LDH layers in order to allow the extraction of phenols from solutions [51]. In the field of phosphors, Yan et *al.* succeeded in intercalating SRB molecules by adjusting the basal spacing with Dodecylbenzenesulfonate (DBS) molecules [50]. We and co-workers, as in many other works, used Sodium Dodecylsulfate (SDS) as a surfactant to allow the best

intercalation of SRB molecules and to obtain the best possible optical properties [15]. Indeed, in both cases, these types of monofunctional surfactants with long alkyl chains allow not only sufficient spacing for an optimal diffusion of the SRB molecules through the LDH interlayer space, but also provide a non-polar environment for them between the LDH layers in order to avoid their aggregation. However, these surfactants suffer from a relatively low thermal stability, which leads to their degradation and to the subsequent delamination of the LDH layers at high temperatures. While many applications are based on this delamination [40,52,53], in the field of the intercalation of dyes in LDH this phenomenon must be absolutely avoided in order to guarantee the confinement of the molecules and avoid their migration and mutual aggregation. Thermally resistant spacers are able to prevent such potential delamination and are therefore of great interest in addressing this issue. A solution is to use bifunctional molecules capable of establishing bonds between two successive stacked LDH layers and thus forcing them to keep this relative position without any possible delamination. This phenomenon, called the pillaring effect, has been extensively studied using terephthalate (TA) as an interleaved anion for various applications [39,54–58.] We and co-workers were the only ones to try to use this anion as a spacer to host SRB molecules between LDH layers, but it led to unsatisfactory results in terms of the resulting optical properties [59].

In the present study, several Zn_2Al LDH structures with the co-intercalation of SRB and spacers were prepared by co-precipitation. The cyclic diacid spacer and the SRB content were varied in order to investigate the influence of these parameters. Structural and optical characterizations of the different samples enabled us to achieve an optimized red-emitting RE-free phosphor with a high absolute photoluminescent quantum yield ($PLQY_{abs}$). Finally, these

latter were incorporated in silicone to prepare luminescent composite films, and thermal stability tests were performed to assess their potential use in LED devices.

2. EXPERIMENTAL SECTION

2.1. Materials

Sulforhodamine B acid form $C_{27}H_{30}N_2O_7S_2$ (laser grade, dye content 95%), Aluminium nitrate nonahydrate $Al(NO_3)_3.9H_2O$ (purity 99.9%), Zinc nitrate hexahydrate $Zn(NO_3)_2.6H_2O$ (purity 99.9%), Benzene-1,4-dicarboxylic acid C_6H_4-1,4-$(CO_2H)_2$ (purity 98%) hereafter called TA, p-Phenylenediacetic acid C_6H_4-1,4-$(CH_2CO_2H)_2$ (purity 97%) hereafter called PAA, p-Phenylenedipropionic acid C_6H_4-1,4-$(CH_2CH_2CO_2H)_2$ (purity 98%) hereafter called PPA and Sodium hydroxide NaOH (purity >98%) were purchased from Sigma-Aldrich and used as received. The silicone-making kit, Bluesil RTV 141 part A and part B, was purchased from Elkem.

2.2. Synthesis of the LDH composites powders

The Zn_2Al-spacer-SRB materials (Spacer = TA, PAA or PPA), named ZNAL-Spacer-SRBx (where x is the SRB molar percentage to compensate the positive charges) were prepared by coprecipitation. Experimentally, to obtain the $[Zn_2Al(OH)_6]^+[Spacer^{2-}]_{(1-x)/2}[SRB^-]_x.mH_2O$, a 50 mL aqueous solution of Zn^{2+} (6.4 mmol) and Al^{3+} (3.2 mmol) was added dropwise to 50 mL of an aqueous solution containing SRB (x%) and ((100-x%)/2) of spacer for 3 hours while stirring. A NaOH solution (0.5 M) enabled the pH to be maintained at 9, and the system was placed in a nitrogen atmosphere at room temperature. The resulting slurry was centrifuged at 4500 rpm and water-cleaned several times. The paste was dried overnight in an oven at 40°C and was then ground to produce a homogeneous powder. As an example, ZNAL-PPA-SRB012 refers to a

composition with x = 0.12 mol% of SRB and 99.88 mol% of PPA spacer. References of all the samples are compiled in Table S1.

2.3. Preparation of the LDH composite films

The silicone/hybrid composite material was made by mixing the LDH powder with part A of the silicone elastomer using a Thinky Mixer mechanical mixer for 10 min at 1200 rpm. The mixture obtained was then passed through a rolling mill (EXAKT brand) composed of three rollers (spacing of 15 μm between the first two rollers and 5 μm between the last two rollers) to achieve a better homogeneity and dispersion of the LDH platelets. Part B was then added at 10 phr and homogenised using the mechanical mixer for 10 min at 1200 rpm. The composite films were prepared by deposition on a Teflon surface using an Elcometer 4340 automatic film applicator. The knife blade height was set to 200 μm and the casting speed was 30 mm/s. The silicone film was cured at 70°C for 2 hours to allow part A and B to react together in order to perform the cross-linking silicone reaction. When the reaction was complete, the film thickness was measured using an Elcometer 456 coating thickness gauge. Three films were obtained with respectively a 10, 20 and 40 wt. % loading of powder. The thickness was found to be around 120 μm in each case.

2.4. Characterisation

X-ray diffraction: LDH powders were analysed by X-ray diffraction using a Philips X-Pert Pro diffractometer in Bragg-Brentano configuration equipped with a Cu-Kα source (30 mA; 40 kV; λ=1.5418 Å). Measurements were performed in a 2Θ range from 2.5° to 70° with a step size of 0.0334°.

Inductively Coupled Plasma mass spectrometry: Quantification of Aluminum and Zinc elements in LDH matrices was performed using an Agilent 5800 ICP-OES Optical Emission Spectrometer.

Emission spectra and luminescence decays: Emission spectra and luminescence decays were recorded at room temperature using the same setup. A laser diode emitting at 375 nm with a repetition rate of 2 MHz and a pulse duration of 65 ps was used as the excitation source. The emitting signal was focused on the slit of a 300 mm focal length monochromator coupled with a photomultiplier.

Photoluminescence quantum yield: Photoluminescence quantum yields of the samples were recorded using a Spectralon coated integrating sphere C9920-02G ($Ø_{int}$ = 76.2 mm) from Hamamatsu Photonics. The source was a Xenon lamp (150 W) equipped with a monochromator, and the spectral measuring system was a Hamamatsu Photonic Multi-channel Analyzer PMA-12.

UV-visible absorption: UV-Visible absorption spectra of the supernatant from the reaction medium and wash waters of LDH composites were recorded using a Horiba Duetta Fluorescence and Absorbance spectrometer.

Quantification of SRB rate remaining in supernatants: To estimate the amount of SRB in supernatants, these latter were analysed by measuring their absorbance at 566 nm, which was the wavelength of maximum absorbance attributed to the S0-S1 absorption of monomers and aggregated forms of SRB [15,50]. By comparing these absorbances with those of a calibration line obtained with aqueous standard solutions of SRB ([SRB] = 0.0625; 0.125; 0.250; 0.5; 0.75; 1; 1.25; 1.5; 1.75; 2; 2.5; 3.5; 5; 7.5; 10 and 15 mg/L) it was possible to determine the SRB concentration remaining in the supernatants (Figure S1 and Table S2). The difference enabled us to calculate the actual amount of SRB dye in the powder.

Thermogravimetric analysis: Thermogravimetric analysis (TGA) was performed using a PerkinElmer TGA 4000 at a heating rate of 5°C/min under nitrogen flow (20.0 mL/min).

Thermogravimetric and mass-spectrometric analysis: Thermogravimetric analysis coupled to mass spectroscopy was performed with a Setaram SETSY evolution thermogravimeter at a heating rate of 5°C/min under air flow (25 mL/min) equipped with a Balzers Thermostar mass spectrometer.

3. RESULTS AND DISCUSSION

3.1. Choice of spacer

3.1.1. Structural characterisation

Three syntheses were carried out with different spacers, TA, PAA or PPA (Figure S2), taking a 0.2 mol% rate of SRB in the LDH composite corresponding to a previously-determined optimized composition [15]. The XRD patterns from 2° to 70° in 2Θ of the ZNAL-Spacer-SRB02 powders are presented in Figure 1.

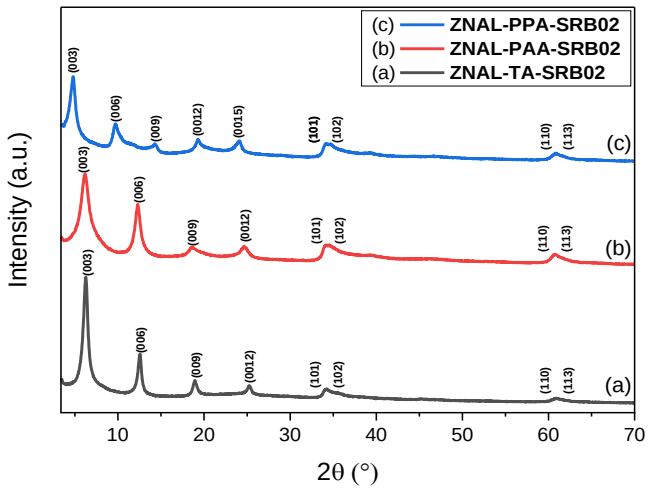

Figure 1. X-ray diffraction patterns of (a) ZNAL-TA-SRB02; (b) ZNAL-PAA-SRB02 and (c) ZNAL-PPA-SRB02.

The three samples were organized in a layered structure, with (00ℓ) harmonic diffraction peaks and reflections at around 35° and 61° in 2Θ related to (101) and (110) peaks describing the LDH structure, as widely reported in the literature [37]. The Zn/Al ratio of 2 was confirmed by the constant cell parameter $a = 2d_{110} = 0.306$ nm calculated for all the samples [60]. We also performed an analysis by Inductively Coupled Plasma mass spectrometry highlighting a ratio of 1.97 Zn for 1 Al. Experimental basal spacing d for each sample was calculated by averaging distances obtained with the positions of the (003), (006) and (009) diffractions peaks by using Bragg's law (1).

$$n\lambda = 2d\ sin\theta \quad \textbf{(1)}$$

Results are summarized in Table 1.

Table 1. Expected and observed basal spacings for ZNAL-Spacer-SRB02 samples

Spacer	Basal spacing d (nm)		Tilt of the spacer (°)[a]
	Expected	Observed	
TA	1.38	1.39	0
PAA	1.57	1.44	≈ 23
PPA	1.87	1.85	≈ 8

These values include the layer thickness of about 0.5 nm.
with e the thickness of a layer and L the length of the spacer

For the ZNAL-TA-SRB02 sample, the basal spacing was found to be 1.39 nm, in accordance with what was expected for a ZNAL-TA phase [54,61]. Theoretical basal spacing for ZNAL-PAA-SRB02 and ZNAL-PPA-SRB02 was calculated to be 1.57 nm and 1.87 nm respectively [61], whereas 1.44 nm and 1.85 nm were determined respectively from experimental measurements. The substantial difference observed for ZNAL-PAA-SRB02 shows that the PAA

spacer is arranged between two LDH layers in an inclined way, as illustrated in Figure 2.

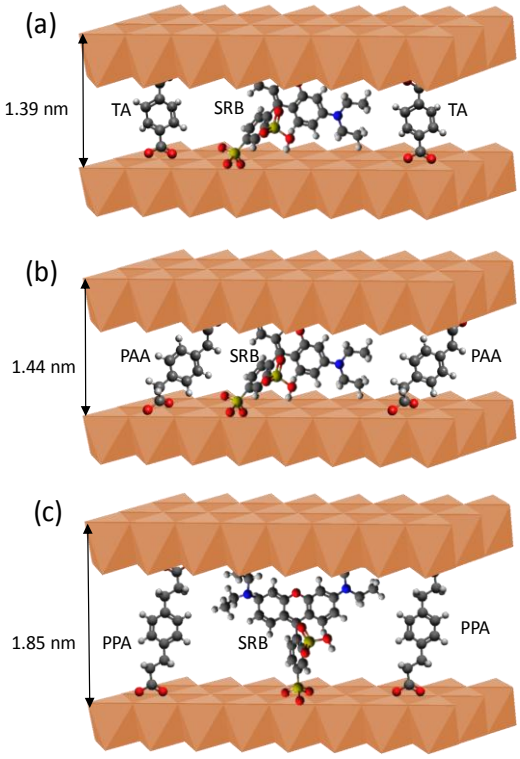

Figure 2. Schematic representation of the ZNAL-Spacer-SRB02 composite with (a) TA spacer; (b) PAA spacer and (c) PPA spacer.

Indeed, theoretical determination of basal spacing assumes that the spacer is perpendicular to the LDH layers (Figure S3). While TA seems not to be inclined, PAA is shown to be inclined by 23° and PPA by 8°.

3.1.2. Thermal stability of the ZNAL-Spacer-SRB powders

A previous study showed that the SRB molecule is stable up to 220°C [59]. Thermogravimetric analysis of the ZNAL-Spacer-SRB02 powders (Figure 3a) as well as thermogravimetric and mass-spectrometric analysis (Figure 3b) of the powder containing PPA, which is the least stable spacer, as highlighted in Figure 3c, shows an initial mass loss below 100°C, attributed to water molecules present at the surface of the LDH layers.

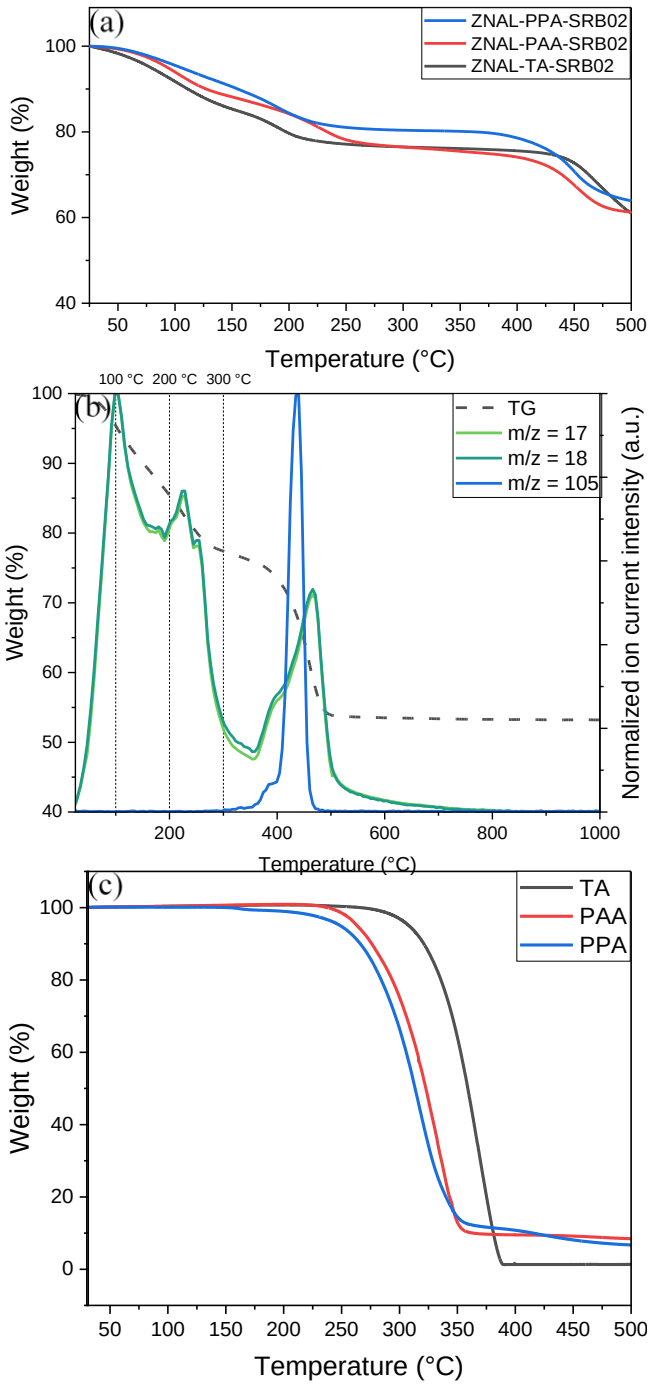

Figure 3. Thermogravimetric analysis of (a) the three ZNAL-Spacer-SRB02 powders; (b) the ZNAL-PPA-SRB02 powder coupled with mass spectrometry and (c) the three pristine spacers.

We can then observe a mass loss starting at around 200°C, attributed to water molecules confined between the LDH layers without affecting the LDH structure. A third mass loss at around 400°C is assigned to the dehydroxylation of the LDH layers, which leads to a degradation of the structure concomitant with the decomposition of the organic anion [62]. Indeed, we do not observe organic mass loss until 300°C, when we detect a main mass loss corresponding to the PPA spacer (m/z = 105), resulting in a possible delamination of the LDH composite. For reasons of clarity, the other organic masses detected (m/z) after 350 °C are not displayed but can be seen in Figure S4.

3.1.3. Effect of the spacer on the dye rate intercalation.

As shown previously, the LDH layers can be spaced from 1.39 nm up to 1.85 nm, which is theoretically sufficient to host the SRB molecule, whose size is between 1 nm and 1.4 nm depending on its orientation (Figure S5). However, the water of the reaction medium as well as the wash waters (referred to as supernatants) of the LDH composites are more or less coloured depending on the spacer used, as seen in Figure 4.

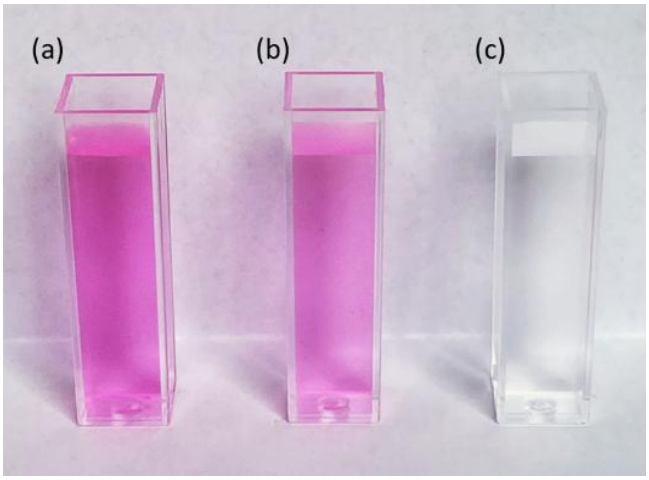

Figure 4. Supernatants after syntheses of ZNAL-Spacer-SRB02 samples with (a) TA spacer; (b) PAA spacer and (c) PPA spacer.

The intense pink coloration of these supernatants for syntheses involving TA and PAA spacers indicates that a significant amount of SRB dye did not diffuse between the LDH sheets and therefore did not intercalate within the LDH matrix. The quantity of SRB molecules added during LDH synthesis being very low (0.2 mol%), it is complicated to directly determine the real SRB amount intercalated between the layers. To quantify this amount, the method explained in experimental section is implemented. Thus, by using TA as a spacer, absorbance of the supernatants reveals that 96% of SRB dye remained in the liquid, meaning that only 4% of SRB dye was well intercalated between LDH layers, whereas 32% of SRB dye was intercalated by using PAA as spacer. Finally, PPA, which is the longest spacer, allowed more than 99% of the SRB dye to be intercalated between the LDH layers. The presence of SRB molecules on the LDH platelets should be discarded, since successive washing steps were employed. This fact shows that we can control the loading of a molecule guest inside a LDH matrix by modulating the interlayer spacing via the use of various anionic spacers. It is important to mention that such an analysis of the "real" amount of incorporated dye molecule is barely reported in the literature. In the present case, it is crucial to know the correct quantity of interleaved SRB molecules in order to better understand their properties and to reach the best optical response. For this purpose, the PPA molecule is chosen as the spacer in the following.

3.2. Optimization of the SRB content in LDH-PPA

3.2.1. Structure of the LDH composites

The previous optimization leading to a SRB rate of 0.2 mol% was carried out on LDH composites using DS as spacer [15]. Here the optimized rate was expected to be different from DS, as co-intercalated PPA dicarboxylate anions have a π-cycle. In order to know the SRB rate producing the best optical properties, several samples using PPA spacers were prepared with

varying SRB amounts (mol%SRB = 0.05; 0.08; 0.1; 0.12; 0.15 and 0.2 mol%). Titration of the supernatants using the calibration line presented in Figure S1 showed that 99% of SRB dye was embedded in each LDH powder. X-ray diffraction patterns are presented in Figure 5 (unbroken lines).

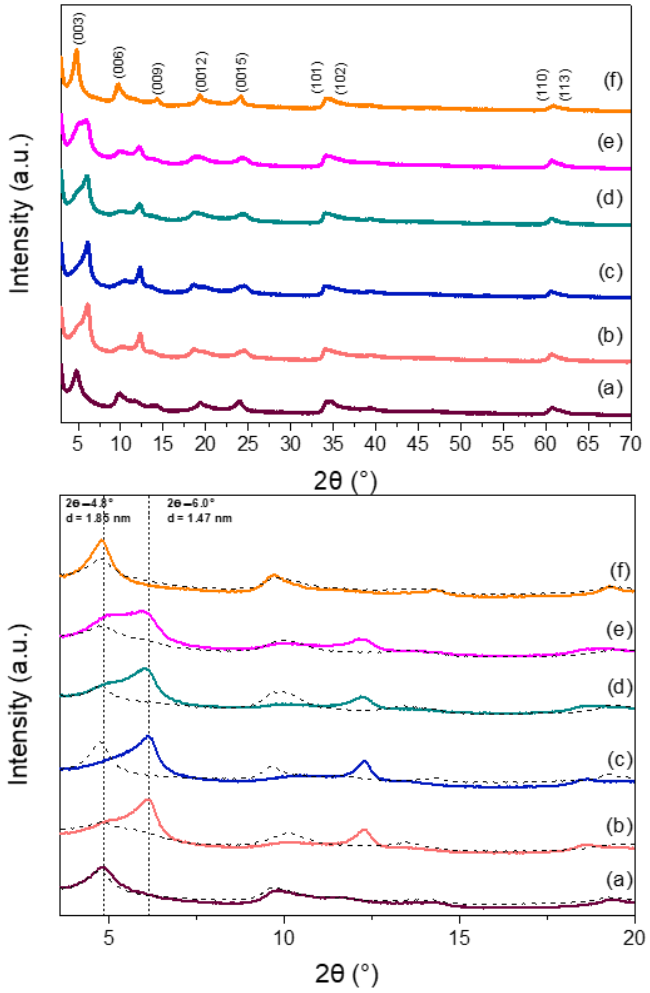

Figure 5. X-ray diffraction patterns from 2.5° to 70° in 2θ (top) and from 3.6° to 20° in 2θ (below) of (a) ZNAL-PPA-SRB005; (b) ZNAL-PPA-SRB008; (c) ZNAL-PPA-SRB01; (d) ZNAL-PPA-SRB012; (e) ZNAL-PPA-SRB015 and (f) ZNAL-PPA-SRB02. Dotted lines represent the X-ray diffraction patterns of the samples 6 months after their synthesis.

A classic LDH structure can be observed for each sample, with the characteristic (00l) harmonic peaks and reflections around 35° and 61° in 2Θ. However, the XRD patterns vary between the different powders. Indeed, depending on the sample, we can observe the presence of two phases: the first as expected, with a (003) peak located at 4.8° in 2Θ leading to a basal spacing of 1.85 nm; and a second with a diffraction peak located at 6° in 2Θ, which can be attributed to a new stacking of the LDH layers with a basal spacing of 1.47 nm. X-ray diffractograms b, c, d and e in Figure 5 illustrate the coexistence of these two phases (d = 1.85 nm and d = 1.47 nm) in various proportions, depending on the sample considered. A similar phenomenon was already observed by Newman *et al.* with the intercalation of terephthalate anions in a MgAl layered double hydroxide [55]. These two phases are due to the different hydration rates of the LDH, which influence the position of the interleaved anion. Thus, a low hydration rate leads to an almost horizontal position of the anion while a high hydration rate forces the latter to position itself perpendicular to the layers. This result demonstrates that the samples did not all contain the same number of interleaved water molecules after synthesis. These same samples were analysed again by X-ray diffraction six months later, and the diffractograms are presented in Figure 5 as dotted lines. As seen, every sample contains only the majority of the first phase (d = 1.85 nm) after a long post-synthesis period, confirming the relatively high hygroscopic character of the LDH matrix, which naturally rehydrates over time.

3.2.2. Optical properties of the powders.

Emission spectra of each sample were recorded from 550 to 750 nm under UV excitation (375 nm) and are presented in Figure 6.

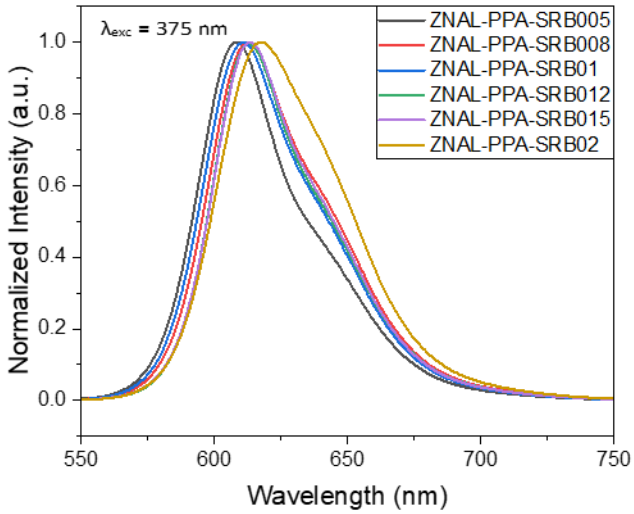

Figure 6. Emission spectra of the ZNAL-PPA-SRB powders recorded under excitation at 375 nm.

As previously shown for similar systems, LDH-PPA-SRB emits over a wide range of wavelengths. The broad asymmetric emission band is characterized by a main emission peak centred around 610 nm attributed to monomer forms of SRB molecules, while the shoulder around 640 nm is attributed to aggregates forms of SRB molecules [50]. When the concentration in SRB is increased, the main peak emission is red-shifted from 608 nm for the sample with the lowest SRB rate to 619 nm for the one with the highest SRB rate, and the shoulder's intensity increases. Such a result arises from the aggregation of SRB into H (face-to-face) and J (end-to-end) forms. According to the exciton theory, H-type aggregates do not lead to luminescence, unlike J-type aggregates [63]. The phenomenon is due to a difference of energy levels in the Jablonski diagram between the two forms of aggregation (Figure 7).

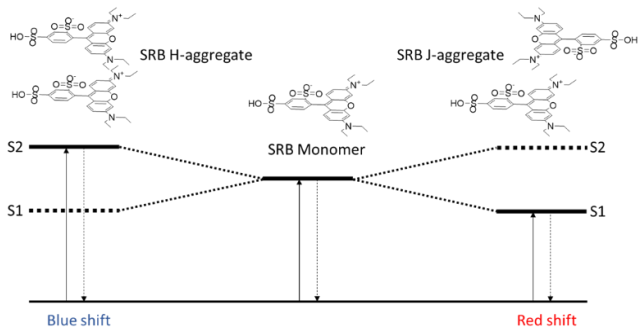

Figure 7. Proposed energy level diagram for SRB molecule.

Compared to the monomer, the H-type aggregate gives rise to a higher energy level, whereas the J-type aggregate leads to a lower energy level, explaining the red shift observed with the increase in SRB concentration. In our samples, the distribution of SRB molecules attached on either side of the LDH layers facing each other and their inclination both favour J-type aggregation instead of H-type. Photoluminescence Quantum Yield (PLQY) measurements allowed us to define the optimum SRB content in our ZNAL-PPA-SRB powders. Indeed, with the aim of obtaining the best optical performances possible, the optimum content will be associated with the highest absolute PLQY. Internal PLQY ($PLQY_{int}$) and Absorption coefficient (Abs) are measured and plotted in Figure 8 between 300 and 600 nm excitation wavelengths.

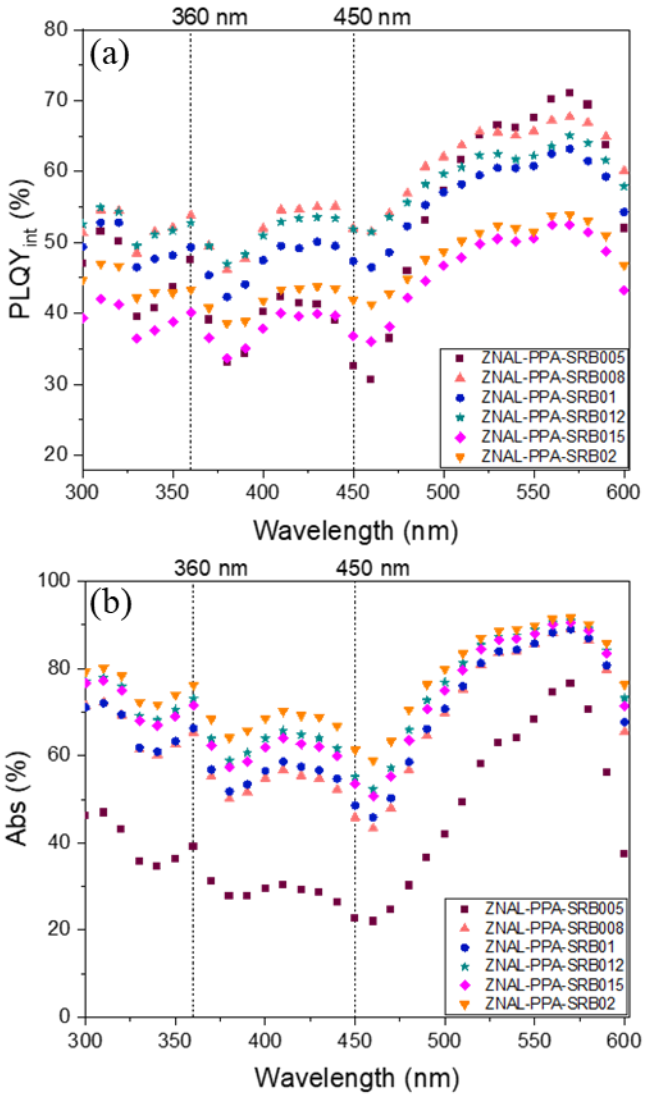

Figure 8. (a) Internal PLQY and (b) absorption coefficient of the ZNAL-PPA-SRB powders for excitation wavelengths from 300 to 600 nm.

PLQY$_{int}$ is defined by: $PLQY_{int} = \frac{number\ of\ emitted\ photons}{number\ of\ absorbed\ photons}$ **(2)**

Abs is defined by: $Abs = \frac{number\ of\ absorbed\ photons}{number\ of\ incident\ photons}$ **(3)**

PLQY$_{int}$ data (Figure 8a) show similar profiles regardless of the SRB rate in the powders studied. However, it should be noted that over the spectral range studied, the lowest PLQY$_{int}$ values are recorded for the powders with the lowest SRB rate (ZNAL-PPA-SRB005) or the

highest SRB rate (ZNAL-PPA-SRB02). This can be explained in the first case by a low number of emitting centres and in the second case by an excessive number of them, leading to an extinction phenomenon by concentration. With regard to the absorption coefficient Abs (Figure 8b), as expected its value increases with the SRB rate in the powders, and this over the whole spectral range studied. We focused on two excitation wavelengths of interest, corresponding to commercial UV and blue LEDs emitting at 360 and 450 nm respectively. As shown in Figure 8, it is clear that for these two excitation wavelengths, absorption increases steadily with SRB concentration and is maximum for the powder containing 0.2 mol% SRB, while the $PLQY_{int}$ passes through a maximum for the sample containing 0.08 mol% SRB. The best $PLQY_{abs}$ resulting from the product between $PLQY_{int}$ and absorption is obtained with the powder containing 0.12 mol% of SRB, and reaches values of 39% and 30% for the two wavelengths, respectively (Figure 9).

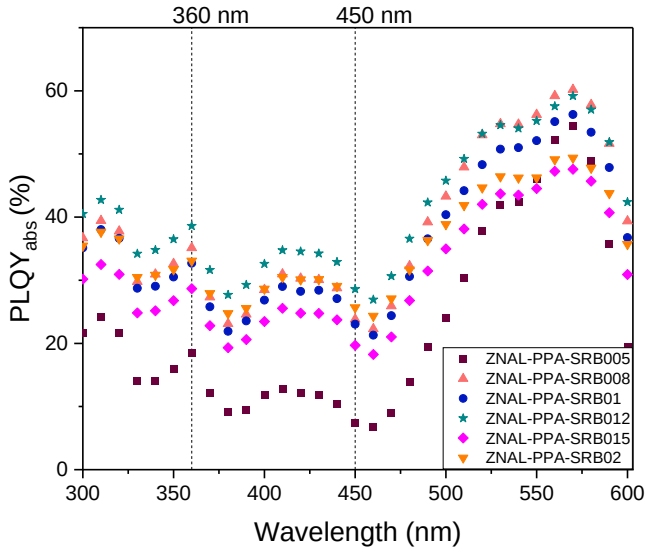

Figure 6. Absolute PLQY of the ZNAL-PPA-SRB powders for excitation wavelengths from 300 to 600 nm.

$PLQY_{abs}$ is defined by : $PLQY_{abs} = PLQY_{int} * Abs$ **(4)**

For this sample, in the 300-600 nm spectral range, values above 27% are recorded, even reaching 60% for 570 nm excitation. The 0.12 mol% SRB rate is thus chosen in the following.

3.2.3. Fluorescence decays

SRB fluorescence decays were studied in solution (10^{-5} M) and a ns range lifetime was measured. Only a few papers report the lifetime of SRB in lamellar structures like LDH [50,64]. In these works, the interest of the spacer to enable the intercalation of the SRB molecule is discussed, but the interpretation of the multi-exponential decay often remains questionable. Indeed, Yan *et al*. explain the bi-exponential decay of luminescence by proposing two interpretations: 1) the SRB molecules are either intercalated in the interlamellar space (for the longest luminescence lifetime), or adsorbed on the surface of the platelets (for the shortest lifetime); 2) the existence of different conformational isomers of SRB. We and co-workers also studied the intercalation of SRB in another LDH matrix: Zn-AL LDH matrix (Mg-Al for Yan *et al*.) with another spacer, DS (DBS for Yan *et al*.) and concluded like Yan *et al.* that the phenomenon was due to the presence of SRB on and within the platelets. Here, as we have highlighted, the totality of the SRB is inside the interlamellar space. In order to understand the interactions between SRB molecules in the interlamellar space, fluorescence decays were recorded (λ_{em} = 646 nm and λ_{exc} = 375 nm) for the different SRB concentrations studied (Figure 10).

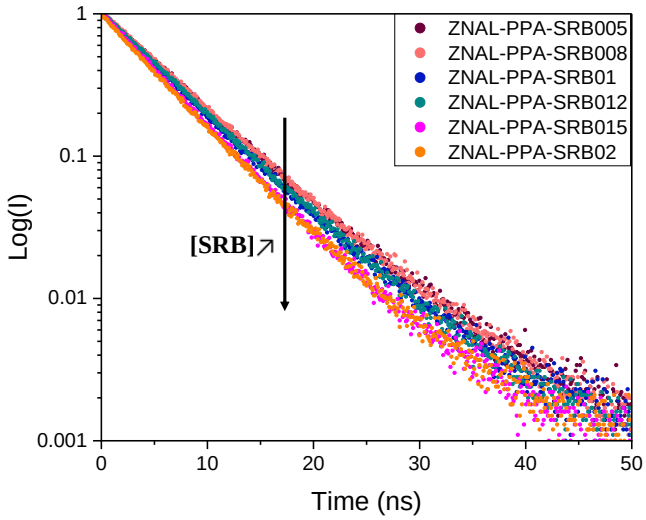

Figure 70. Luminescence decay profiles of the ZNAL-PPA-SRB powders (excitation at 375 nm and emission at 646 nm).

The semi-logarithmic representation of the decays recorded at 300K highlights the non-monoexponential nature of the fluorescence decay. Luminescence lifetimes are obtained by fitting the decay profiles with a double exponential function. The logarithmic decay profiles and fits for the ZNAL-PPA-SRB005 and ZNAL-PPA-SRB02 powders (the powders with the lowest and the highest SRB rates respectively) are presented in Figure S6. The derived time constants from the fit of all the powders studied are reported in Table 2.

Table 2. Time constants recorded for all the ZNAL-PPA-SRB powders studied (λ_{em} = 646 nm and λ_{exc} = 375 nm)

	τ_1	A_1	τ_2	A_2	$<\tau>$	R^2
ZNAL-PPA-SRB005	6.1	0.91	9.8	0.09	6.4	0.999050
ZNAL-PPA-SRB008	6.3	0.86	9.9	0.14	6.8	0.999120
ZNAL-PPA-SRB01	6.1	0.84	9.2	0.16	6.6	0.999348

ZNAL-PPA-SRB012	5.6	0.84	9.3	0.16	6.2	0.999100
ZNAL-PPA-SRB015	5.2	0.78	8.2	0.22	5.9	0.999999
ZNAL-PPA-SRB02	5.0	0.75	8.3	0.25	5.8	0.999800
SRB in aqueous solution 1.10^{-8} mol.L^{-1}	2.0	0.99	12.3	0.01	2.1	0.998850

*A_i (i = 1 or 2) is the percentage of τ_i

Thus, the equation used for the fit is:

$$y(x) = A_1 * \exp\left(-\frac{x}{\tau_1}\right) + A_2 * \exp\left(-\frac{x}{\tau_2}\right) \quad \textbf{(5)}$$

where A_1 and A_2 are the amplitudes of the first and second exponential terms, respectively, and τ_1 and τ_2 are the lifetime constants of the first and second terms, respectively. Figure 11 also shows the recorded fluorescence, under the same conditions (λ_{em} = 646 nm and λ_{exc} = 375 nm) as for the ZNAL-PPA-SRB powders, of SRB in aquous solution for a concentration of 1.10^{-8} mol.L^{-1}, a concentration comparable to that introduced in the ZNAL-PPA-SRB005 powder.

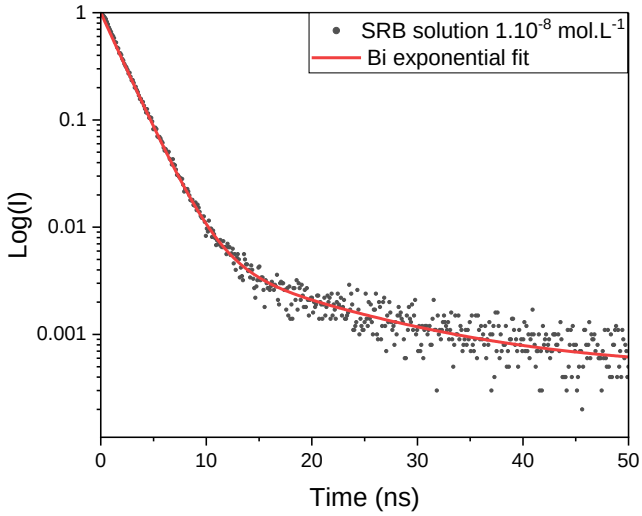

Figure 11. Luminescence decay profile of a SRB solution (excitation at 375 nm and emission at 646 nm).

In this case, the average lifetime <t> obtained is identical to that recorded by Rifani et al [65]. Compared to the aqueous solution of SRB (1.10-8 mol.L-1), the average fluorescence lifetime of ZNAL-PPA-SRB is three time higher. This fluorescence lifetime improvement is probably due to the immobilization of the SRB in the LDH matrix [50]. Moreover, we observe a slight decrease in the average lifetime with the increase in the amount of SRB in the basal spacing (6.4 ns for SRB005 and 5.8 ns for SRB02). This behaviour, already observed by several authors, can be explained by the formation of aggregations, as indicated by the results of emission spectra (Figure 7) [50]. However, both recorded lifetimes for the ZNAL-PPA-SRB are significantly longer than the average lifetime of SRBs in solution. Therefore, based on the published work, we can state that the lifetimes recorded for SRBs in our LDH matrix, for all concentrations studied, reflect a weak aggregation of SRBs in the interlamellar space. The spacer helps to limit the interactions between SRB molecules. Although the decrease in mean lifetime with increasing SRB concentration indicates that the "dilution" role played by the spacer decreases, as expected, when the SRB concentration exceeds a certain concentration, the $PLQY_{abs}$ measurements presented in Figure 9, support the idea that the PPA plays its role perfectly over the studied SRB concentration range. The two lifetimes recorded for SRB in the interlamellar space may be justified by the existence of different conformational isomers of SRB.

3.3. Silicone-LDH composite films (SRB rate = 0.12 mol%)

3.3.1. Integration of the powder in Silicone

In order to facilitate its use and for potential applications in LED devices for instance, the optimized sample, i.e. ZNAL-PPA-SRB012, was incorporated in a Silicone film following the method detailed in the experimental section. Three films of a constant thickness of 120 µm (+/- 5 µm) were prepared with powder fillers of 10, 20 and 40 wt.%, respectively, referred to as Si-

LDH10, Si-LDH20 and Si-LDH40 for reasons of clarity. Figure 12 is a photograph of the three films, under daylight and under UV (365 nm) showing their homogeneous aspect and luminescence properties.

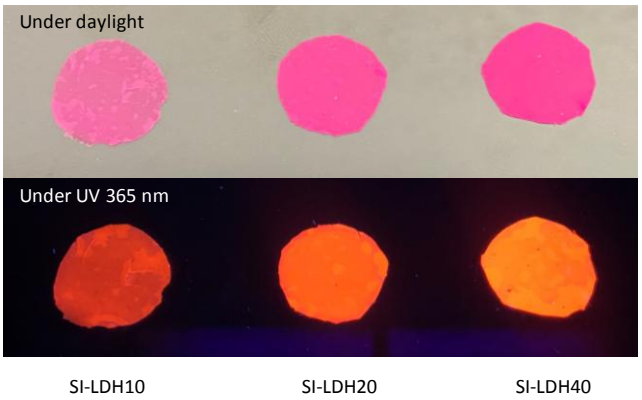

Figure 82. Silicone films under daylight and UV (365 nm).

3.3.2. Optical properties of the composite films

Emission spectra of the films under 360 nm excitation were recorded and compared with those of the ZNAL-PPA-SRB012 powder. Results are shown in Figure 13.

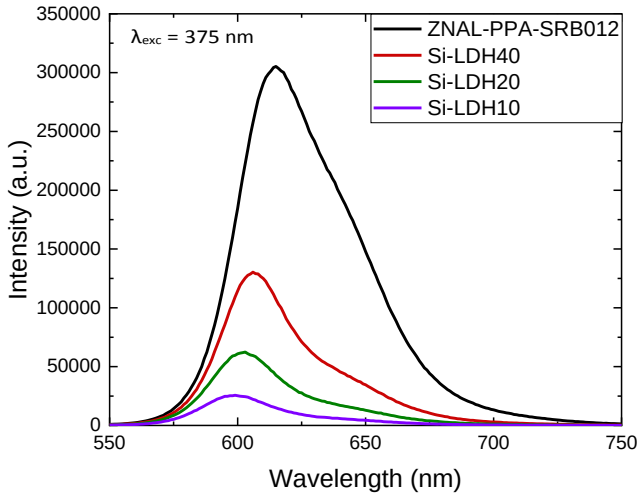

Figure 93. Emission spectra of the three silicone films compared with the LDH powder at 360 nm.

A blue shift can be observed for the films compared to the LDH powder, attributed to a de-agglomeration of the powder when dispersed in Silicone and thus a disaggregation of SRB molecules. This is confirmed by the difference in the ratio between the intensities of the two main peaks. Thus, according to the emission peaks, powder aggregation increases when its loading in Silicone increases. The silicone film loaded with 40 wt.% of powder enables an emission intensity almost as strong as that of the powder to be obtained. The PLQY of the films was measured under excitation from 300 nm to 600 nm, and compared with that of the LDH powder (Figure 14).

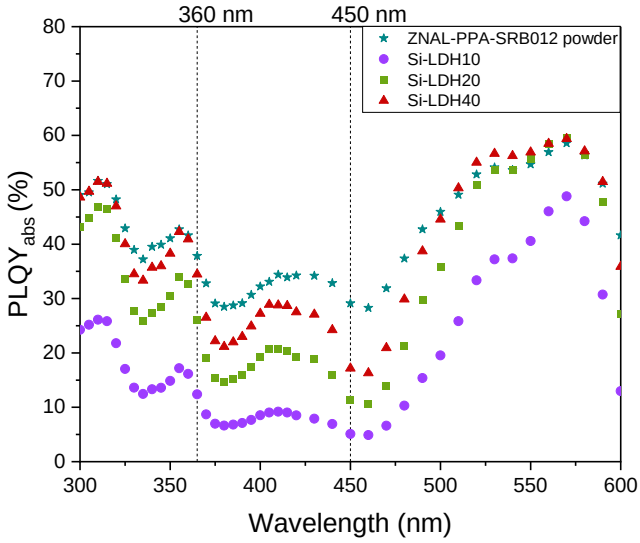

Figure 104. Absolute PLQY of the three silicone films compared with the LDH powder for excitation wavelengths from 300 to 600 nm.

Regardless the film, the dispersion of the powder in silicone induces a decrease in $PLQY_{abs}$ particularly in the 370-480 nm range. Among the three prepared films, the increase in powder loading results in an increase in $PLQY_{abs}$ up to 40 wt.% dispersion, whose film achieves the same optical properties as the powder. Finally, $PLQY_{abs}$ measurements of 40% and 30% are obtained under 360 nm and 450 nm excitation, and a maximum of 60% is reached under 570 nm excitation.

3.3.3. Thermal stability of the silicone films

To be used in a LED device, a phosphor must meet specific standards, such as being stable at various temperatures. The stability of the silicone films loaded with ZNAL-PPA-SRB012 powder (10, 20 and 40 wt. %) was studied by heating them at 85°C and 120°C for 24h. $PLQY_{abs}$ results for the 40 wt.% film before and after the two thermal treatments are presented in Figure 15.

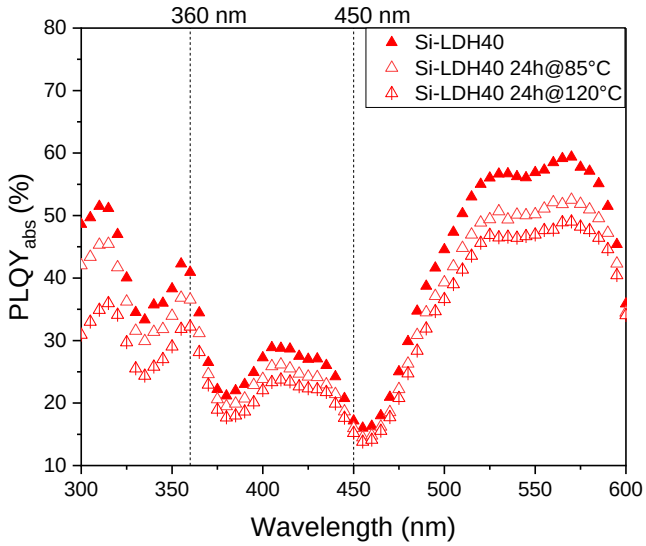

Figure 115. Absolute PLQY of the Si-LDH40 film before and after the heat treatments.

Depending on the excitation wavelength, a greater or lesser loss of yield is observed after heat treatment. We and co-workers demonstrated that the pristine silicone film does not degrade at these temperatures [59], thus any loss in PLQY should be attributed to the LDH powder. Under 360 nm, a relative loss of approximately 3% and 5% only is observed after treatment at 85°C and 120°C respectively. No loss is observed under blue excitation whatever the thermal treatment. If we consider the other excitation wavelengths, the film lost approximately 5% and 10% of $PLQY_{abs}$ after a treatment at 85°C and 120°C, respectively. According to the thermal study of the ZNAL-PPA-SRB samples (Figure 3), no degradation of the powder is expected in this range of temperatures, and as shown before, the dehydration of the composite which occurs around 100°C

does not affect the PLQY. Thus, in agreement with the work we did in the past, the loss of PLQY is certainly due to an aggregation of the luminescent particles inside the silicone film induced by temperature. However, we have to note that the PLQY loss and therefore the aggregation is much lower than that observed in previous works[15], which emphasizes the real benefit of using PPA molecules as a novel spacer instead of classical spacers such as DS. Furthermore, the higher thermal stability of PPA in comparison with DS spacer leads to luminescent composite films exhibiting a weaker loss of the absolute photoluminescent quantum yield upon thermal treatment as illustrated for two silicone films containing 20 wt.% of LDH-PPA-SRB and LDH-DS-SRB powders respectively (Figure S7), before et after heat treatment at 120°C for 24h.

4. CONCLUSIONS

In this work, hybrid organic-inorganic powders were developed involving the co-intercalation of SRB with cyclic di-functionalized molecules as spacers within a LDH structure. These spacers were found to increase the basal spacing between LDH layers and thus to allow an efficient intercalation of SRB molecules within the structure. The importance of matching the size of the spacer was clearly shown by the colour of the supernatant, directly related to the real uptake of SRB molecules. Thus, PPA as a spacer allows more than 99% of SRB to be hosted within the hybrid powder, and its advantage compared to commonly-used spacers (DS, DBS…) arises from the presence of two carboxylate functions pillaring two adjacent LDH sheets. The phenomenon prevents the delamination of the layers and enables the structure hosting the SRB to have good temperature resistance. The SRB rate was optimized at 0.12 mol%, with $PLQY_{abs}$ values between 30% and 60% depending on the excitation wavelength. Photoluminescence decay times for the sample reveal that the dilution state of SRB molecules in LDH is close to that in aqueous solution, although conformational SRB isomers between LDH layers were detected. The optical

properties of the LDH hybrid powders are mostly preserved when they are incorporated into silicone films. Among the films tested, a loading rate of 40 wt. % of powder in silicone leads to the best optical properties. Finally, the film remains highly fluorescent after thermal treatment at 85°C or 120°C, opening up its possible use in LED devices.

ASSOCIATED CONTENT

Supporting Information. The following files are available free of charge.

A table with all the LDH samples references, the absorbance calibration line for the titration of supernatants, the determination of SRB rate intercalated between LDH layers, the structures of the spacers, the theoretical basal spacing calculation for each spacers, the thermogravimetric and mass spectrometry of samples, the structure of SRB molecule and the luminescence decay profiles of the samples are presented in supporting information (PDF).

AUTHOR INFORMATION

Corresponding Author

*Damien Boyer – Email : damien.boyer@sigma-clermont.fr

Author contributions

Guillaume Zerbib, Damien Boyer, Geneviève Chadeyron, François Réveret and Fabrice Leroux contributed equally.

REFERENCES

(1) Nair, G. B.; Swart, H. C.; Dhoble, S. J. A Review on the Advancements in Phosphor-Converted Light Emitting Diodes (Pc-LEDs): Phosphor Synthesis, Device Fabrication and Characterization. *Progress in Materials Science* **2020**, *109*, 100622. https://doi.org/10.1016/j.pmatsci.2019.100622.
(2) Ricci, P. C. Assessment of Crystalline Materials for Solid State Lighting Applications: Beyond the Rare Earth Elements. *Crystals* **2020**, *10* (7), 559. https://doi.org/10.3390/cryst10070559.
(3) Sato, M.; Kim, S. W.; Shimomura, Y.; Hasegawa, T.; Toda, K.; Adachi, G. Rare Earth-Doped Phosphors for White Light-Emitting Diodes. In *Handbook on the Physics and Chemistry of Rare Earths*; Elsevier, 2016; Vol. 49, pp 1–128. https://doi.org/10.1016/bs.hpcre.2016.03.001.
(4) Hoerder, G. J.; Seibald, M.; Baumann, D.; Schröder, T.; Peschke, S.; Schmid, P. C.; Tyborski, T.; Pust, P.; Stoll, I.; Bergler, M.; Patzig, C.; Reißaus, S.; Krause, M.; Berthold, L.; Höche, T.; Johrendt, D.; Huppertz, H. Sr[Li2Al2O2N2]:Eu2+—A High Performance Red Phosphor to Brighten the Future. *Nat Commun* **2019**, *10* (1), 1824. https://doi.org/10.1038/s41467-019-09632-w.
(5) Park, J. Y.; Yang, H. K. Development of Red-Emitting La2ZnTiO6:Eu3+ Phosphors for WLED and Visualization of Latent Fingerprint Applications. *Materials Today Communications* **2022**, *31*, 103391. https://doi.org/10.1016/j.mtcomm.2022.103391.
(6) Kishore Babu, J.; Sridhar, M.; Sai Prasad, A. S.; Patrick, G.; Suresh, K. Novel Red Phosphor for LED Applications. *Materials Today: Proceedings* **2021**, *44*, 294–299. https://doi.org/10.1016/j.matpr.2020.09.468.
(7) Génois, R.; Jobic, S.; Ouvrard, G.; Massuyeau, F.; Gautier, R. The Crucial Impact of Cerium Reduction on Photoluminescence. *Applied Materials Today* **2020**, *20*, 100643. https://doi.org/10.1016/j.apmt.2020.100643.
(8) Xie, F.; Zhang, T. A.; Dreisinger, D.; Doyle, F. A Critical Review on Solvent Extraction of Rare Earths from Aqueous Solutions. *Minerals Engineering* **2014**, *56*, 10–28. https://doi.org/10.1016/j.mineng.2013.10.021.
(9) Ganguli, R.; Cook, D. R. Rare Earths: A Review of the Landscape. *MRS Energy & Sustainability* **2018**, *5* (1), 6. https://doi.org/10.1557/mre.2018.7.
(10) Tkaczyk, A. H.; Bartl, A.; Amato, A.; Lapkovskis, V.; Petranikova, M. Sustainability Evaluation of Essential Critical Raw Materials: Cobalt, Niobium, Tungsten and Rare Earth Elements. *J. Phys. D: Appl. Phys.* **2018**, *51* (20), 203001. https://doi.org/10.1088/1361-6463/aaba99.
(11) Lukowiak, A.; Zur, L.; Tomala, R.; LamTran, T. N.; Bouajaj, A.; Strek, W.; Righini, G. C.; Wickleder, M.; Ferrari, M. Rare Earth Elements and Urban Mines: Critical Strategies for Sustainable Development. *Ceramics International* **2020**, *46* (16), 26247–26250. https://doi.org/10.1016/j.ceramint.2020.03.067.
(12) Breton, T. Critical Raw Materials Act: Securing the New Gas & Oil at the Heart of Our Economy I Blog of Commissioner Thierry Breton. *European Commission Statement/22/5523* **2022**, No. Statement/22/5523.
(13) Cathalan, J.; Salaün, M.; Gaffuri, P.; Potdevin, A.; Réveret, F.; Ibanez, A.; Chadeyron, G.; Gautier-Luneau, I. Optimization of the Pechini-Derived Synthesis of Rare-Earth Free Aluminum Borate Phosphors Presenting Tunable White Emission. *J Mater Sci* **2022**, *57* (33), 15829–15842. https://doi.org/10.1007/s10853-022-07619-5.
(14) Bharat, L. K.; Jeon, S.-K.; Krishna, K. G.; Yu, J. S. Rare-Earth Free Self-Luminescent Ca2KZn2(VO4)3 Phosphors for Intense White Light-Emitting Diodes. *Sci Rep* **2017**, *7* (1), 42348. https://doi.org/10.1038/srep42348.
(15) Legentil, P.; Leroux, F.; Therias, S.; Boyer, D.; Chadeyron, G. Sulforhodamine B-LDH Composite as a Rare-Earth-Free Red-Emitting Phosphor for LED Lighting. *J. Mater. Chem. C* **2020**, *8* (34), 11906–11915. https://doi.org/10.1039/D0TC02802A.
(16) Vichai, V.; Kirtikara, K. Sulforhodamine B Colorimetric Assay for Cytotoxicity Screening. *Nat Protoc* **2006**, *1* (3), 1112–1116. https://doi.org/10.1038/nprot.2006.179.

(17) Keepers, Y. P.; Pizao, P. E.; Peters, G. J.; van Ark-Otte, J.; Winograd, B.; Pinedo, H. M. Comparison of the Sulforhodamine B Protein and Tetrazolium (MTT) Assays for in Vilro Chemosensitivity Testing.
(18) Jones, W. K. Water Tracing in Karst Aquifers. In *Encyclopedia of Caves*; Elsevier, 2019; pp 1144–1155. https://doi.org/10.1016/B978-0-12-814124-3.00134-5.
(19) Johansen, K.; Dunne, A. F.; Tu, Y.-H.; Almashharawi, S.; Jones, B. H.; McCabe, M. F. Dye Tracing and Concentration Mapping in Coastal Waters Using Unmanned Aerial Vehicles. *Sci Rep* **2022**, *12* (1), 1141. https://doi.org/10.1038/s41598-022-05189-9.
(20) Gosetti, F.; Bolfi, B.; Marengo, E. Identification of Sulforhodamine B Photodegradation Products Present in Nonpermanent Tattoos by Micro Liquid Chromatography Coupled with Tandem High-Resolution Mass Spectrometry. *Anal Bioanal Chem* **2015**, *407* (16), 4649–4659. https://doi.org/10.1007/s00216-015-8667-5.
(21) Bravo, E. The Forensic Analysis of Children's Temporary Tattoos. **2019**.
(22) Opinion on Acid Red 52. *Scientific Committee on Consumer Products* **2008**.
(23) Ma, X.; Sun, R.; Cheng, J.; Liu, J.; Gou, F.; Xiang, H.; Zhou, X. Fluorescence Aggregation-Caused Quenching versus Aggregation-Induced Emission: A Visual Teaching Technology for Undergraduate Chemistry Students. *J. Chem. Educ.* **2016**, *93* (2), 345–350. https://doi.org/10.1021/acs.jchemed.5b00483.
(24) Zhang, Q.; Feng, Y.; Valleix, R.; Chadeyron, G.; Boyer, D.; Leroux, F. Co-Assembled Photoactive Organic Molecules into Layered Double Hydroxide as Fluorescent Fillers for Silicone Films. *Materials Today Communications* **2021**, *28*, 102479. https://doi.org/10.1016/j.mtcomm.2021.102479.
(25) Li, B.; Jiang, W.; Xu, Y.; Xu, Z.; Yan, Q.; Yong, G. Dyes Encapsulated in a Novel Flexible Metal–organic Framework Show Tunable and Stimuli-Responsive Phosphorescence. *Dyes and Pigments* **2020**, *174*, 108017. https://doi.org/10.1016/j.dyepig.2019.108017.
(26) Sun, Z.; Khurshid, A.; Sohail, M.; Qiu, W.; Cao, D.; Su, S.-J. Encapsulation of Dyes in Luminescent Metal-Organic Frameworks for White Light Emitting Diodes. *Nanomaterials* **2021**, *11* (10), 2761. https://doi.org/10.3390/nano11102761.
(27) Maity, K.; Mukherjee, D.; Sen, M.; Biradha, K. Fluorescent Dye-Based Metal–Organic Framework Piezochromic and Multicolor-Emitting Two-Dimensional Materials for Light-Emitting Devices. *ACS Appl. Nano Mater.* **2019**, *2* (3), 1614–1620. https://doi.org/10.1021/acsanm.9b00055.
(28) Ogawa, M.; Kuroda, K. Photofunctions of Intercalation Compounds. *Chem. Rev.* **1995**, *95* (2), 399–438. https://doi.org/10.1021/cr00034a005.
(29) Lamouche, G.; Lavallard, P.; Gacoin, T. Optical Properties of Dye Molecules as a Function of the Surrounding Dielectric Medium. *Phys. Rev. A* **1999**, *59* (6), 4668–4674. https://doi.org/10.1103/PhysRevA.59.4668.
(30) Carrasco, J. A.; Sanchis-Gual, R.; Silva, A. S.-D.; Abellán, G.; Coronado, E. Influence of the Interlayer Space on the Water Oxidation Performance in a Family of Surfactant-Intercalated NiFe-Layered Double Hydroxides. *Chem. Mater.* **2019**, *31* (17), 6798–6807. https://doi.org/10.1021/acs.chemmater.9b01263.
(31) Heravi, M. M.; Mohammadi, P. Layered Double Hydroxides as Heterogeneous Catalyst Systems in the Cross-Coupling Reactions: An Overview. *Mol Divers* **2022**, *26* (1), 569–587. https://doi.org/10.1007/s11030-020-10170-7.
(32) Mallakpour, S.; Tabebordbar, H. Layered Double Hydroxide Polymer Nanocomposites for Catalysis. In *Layered Double Hydroxide Polymer Nanocomposites*; Elsevier, 2020; pp 805–834. https://doi.org/10.1016/B978-0-08-101903-0.00020-9.
(33) Ameena Shirin, V. K.; Sankar, R.; Johnson, A. P.; Gangadharappa, H. V.; Pramod, K. Advanced Drug Delivery Applications of Layered Double Hydroxide. *Journal of Controlled Release* **2021**, *330*, 398–426. https://doi.org/10.1016/j.jconrel.2020.12.041.

(34) Johnston, A.-L.; Lester, E.; Williams, O.; Gomes, R. L. Understanding Layered Double Hydroxide Properties as Sorbent Materials for Removing Organic Pollutants from Environmental Waters. *Journal of Environmental Chemical Engineering* **2021**, *9* (4), 105197. https://doi.org/10.1016/j.jece.2021.105197.
(35) Li, Y.; Chen, J.; Cai, P.; Wen, Z. An Electrochemically Neutralized Energy-Assisted Low-Cost Acid-Alkaline Electrolyzer for Energy-Saving Electrolysis Hydrogen Generation. *J. Mater. Chem. A* **2018**, *6* (12), 4948–4954. https://doi.org/10.1039/C7TA10374C.
(36) Shao, M.; Zhang, R.; Li, Z.; Wei, M.; Evans, D. G.; Duan, X. Layered Double Hydroxides toward Electrochemical Energy Storage and Conversion: Design, Synthesis and Applications. *Chem. Commun.* **2015**, *51* (88), 15880–15893. https://doi.org/10.1039/C5CC07296D.
(37) *Layered Double Hydroxides*; Duan, X., Evans, D. G., Eds.; Structure and Bonding; Springer-Verlag: Berlin/Heidelberg, 2006; Vol. 119. https://doi.org/10.1007/b100426.
(38) Sonoyama, N.; Takagi, K.; Yoshida, S.; Ota, T.; Kimilita, P. D.; Ogasawara, Y. Optical Properties of the Europium (II) and (III) Ions Doped Metal Oxides Obtained from Sintering Layered Double Hydroxides, and Their Fine Structures. *Applied Clay Science* **2020**, *186*, 105440. https://doi.org/10.1016/j.clay.2020.105440.
(39) Gao, X.; Lei, L.; Kang, L.; Wang, Y.; Lian, Y.; Jiang, K. Synthesis, Characterization and Optical Properties of a Red Organic–Inorganic Phosphor Based on Terephthalate Intercalated Zn/Al/Eu Layered Double Hydroxide. *Journal of Alloys and Compounds* **2014**, *585*, 703–707. https://doi.org/10.1016/j.jallcom.2013.09.168.
(40) Bai, M.; Liu, X.; Sakai, N.; Ebina, Y.; Jia, L.; Tang, D.; Sasaki, T.; Ma, R. General Synthesis of Layered Rare-Earth Hydroxides (RE = Sm, Eu, Gd, Tb, Dy, Ho, Er, Y) and Direct Exfoliation into Monolayer Nanosheets with High Color Purity. *J. Phys. Chem. Lett.* **2021**, *12* (41), 10135–10143. https://doi.org/10.1021/acs.jpclett.1c03047.
(41) Valleix, R.; Zhang, Q.; Boyer, D.; Boutinaud, P.; Chadeyron, G.; Feng, Y.; Okuno, H.; Réveret, F.; Hintze-Bruening, H.; Leroux, F. A First Wide-Open LDH Structure Hosting InP/ZnS QDs: A New Route Toward Efficient and Photostable Red-Emitting Phosphor. *Adv. Mater.* **2021**, *33* (38), 2103411. https://doi.org/10.1002/adma.202103411.
(42) Cho, S.; Hong, S. C.; Kim, S. Quantum Dot–Layered Double Hydroxide Composites for near-Infrared Emitting Codes. *J. Mater. Chem. C* **2014**, *2* (3), 450–457. https://doi.org/10.1039/C3TC31699H.
(43) Cho, S.; Jung, S.; Jeong, S.; Bang, J.; Park, J.; Park, Y.; Kim, S. Strategy for Synthesizing Quantum Dot-Layered Double Hydroxide Nanocomposites and Their Enhanced Photoluminescence and Photostability. *Langmuir* **2013**, *29* (1), 441–447. https://doi.org/10.1021/la303812y.
(44) Costantino, U.; Coletti, N.; Nocchetti, M.; Aloisi, G. G.; Elisei, F.; Latterini, L. Surface Uptake and Intercalation of Fluorescein Anions into Zn−Al−Hydrotalcite. Photophysical Characterization of Materials Obtained. *Langmuir* **2000**, *16* (26), 10351–10358. https://doi.org/10.1021/la001096d.
(45) Legentil, P.; Leroux, F.; Therias, S.; Mahiou, R.; Chadeyron, G. Revisiting Fluorescein and Layered Double Hydroxide Using a Synergistic Approach: A Complete Optical Study. *Journal of Luminescence* **2019**, *215*, 116634. https://doi.org/10.1016/j.jlumin.2019.116634.
(46) Chakraborty, C.; Dana, K.; Malik, S. Intercalation of Perylenediimide Dye into LDH Clays: Enhancement of Photostability. *J. Phys. Chem. C* **2011**, *115* (5), 1996–2004. https://doi.org/10.1021/jp110486r.
(47) Yan, D.; Lu, J.; Wei, M.; Ma, J.; Evans, D. G.; Duan, X. A Combined Study Based on Experiment and Molecular Dynamics: Perylene Tetracarboxylate Intercalated in a Layered Double Hydroxide Matrix. *Phys. Chem. Chem. Phys.* **2009**, *11* (40), 9200. https://doi.org/10.1039/b907366c.
(48) Bauer, J.; Behrens, P.; Speckbacher, M.; Langhals, H. Composites of Perylene Chromophores and Layered Double Hydroxides: Direct Synthesis, Characterization, and Photo- and Chemical Stability. *Adv. Funct. Mater.* **2003**, *13* (3), 241–248. https://doi.org/10.1002/adfm.200390036.

(49) Yan, L.; Zhou, M.; Zhang, X.; Huang, L.; Chen, W.; Roy, V. A. L.; Zhang, W.; Chen, X. A Novel Type of Aqueous Dispersible Ultrathin-Layered Double Hydroxide Nanosheets for in Vivo Bioimaging and Drug Delivery. *ACS Appl. Mater. Interfaces* **2017**, *9* (39), 34185–34193. https://doi.org/10.1021/acsami.7b05294.
(50) Yan, D.; Lu, J.; Wei, M.; Evans, D. G.; Duan, X. Sulforhodamine B Intercalated Layered Double Hydroxide Thin Film with Polarized Photoluminescence. *J. Phys. Chem. B* **2009**, *113* (5), 1381–1388. https://doi.org/10.1021/jp8084217.
(51) Grover, A.; Kaur, R.; Mohiuddin, I.; Malik, A. K.; Aulakh, J. S.; Tsang, Y. F.; Kim, K.-H. Surfactant-Modified Zn/Al-Layered Double Hydroxides for Efficient Extraction of Alkyl Phenols from Aqueous Samples. *Environmental Research* **2019**, *177*, 108605. https://doi.org/10.1016/j.envres.2019.108605.
(52) Takács, D.; Varga, G.; Csapó, E.; Jamnik, A.; Tomšič, M.; Szilágyi, I. Delamination of Layered Double Hydroxide in Ionic Liquids under Ambient Conditions. *J. Phys. Chem. Lett.* **2022**, *13* (51), 11850–11856. https://doi.org/10.1021/acs.jpclett.2c03275.
(53) Cermelj, K.; Ruengkajorn, K.; Buffet, J.-C.; O'Hare, D. Layered Double Hydroxide Nanosheets via Solvothermal Delamination. *Journal of Energy Chemistry* **2019**, *35*, 88–94. https://doi.org/10.1016/j.jechem.2018.11.008.
(54) Drezdzon, M. A. Synthesis of Isopolymetalate-Pillared Hydrotalcite via Organic-Anion-Pillared Precursors. *Inorg. Chem.* **1988**, *27* (25), 4628–4632. https://doi.org/10.1021/ic00298a024.
(55) Newman, S. P.; Williams, S. J.; Coveney, P. V.; Jones, W. Interlayer Arrangement of Hydrated MgAl Layered Double Hydroxides Containing Guest Terephthalate Anions: Comparison of Simulation and Measurement. *J. Phys. Chem. B* **1998**, *102* (35), 6710–6719. https://doi.org/10.1021/jp981426r.
(56) Arias, S.; Eon, J. G.; San Gil, R. A. S.; Licea, Y. E.; Palacio, L. A.; Faro, A. C. Synthesis and Characterization of Terephthalate-Intercalated NiAl Layered Double Hydroxides with High Al Content. *Dalton Trans.* **2013**, *42* (6), 2084–2093. https://doi.org/10.1039/C2DT31502E.
(57) Cui, W.; Jiao, Q.; Zhao, Y.; Li, X.; Zhou, M.; Shen, H. Preparation of Terephthalate-Intercalated Layered Double Hydroxides Using Mixed Hydroxides. *Synthesis and Reactivity in Inorganic, Metal-Organic, and Nano-Metal Chemistry* **2012**, *42* (4), 579–582. https://doi.org/10.1080/15533174.2011.613888.
(58) Greenwell, H. C.; Jones, W.; Rugen-Hankey, S. L.; Holliman, P. J.; Thompson, R. L. Efficient Synthesis of Ordered Organo-Layered Double Hydroxides. *Green Chem.* **2010**, *12* (4), 688. https://doi.org/10.1039/b916301h.
(59) Legentil, P.; Leroux, F.; Therias, S.; Boyer, D.; Reveret, F.; Chadeyron, G. Reliability Study under Thermal and Photonic Stresses of Sulforhodamine B (SRB) Confined in Layered Double Hydroxide (LDH). *Applied Clay Science* **2021**, *201*, 105922. https://doi.org/10.1016/j.clay.2020.105922.
(60) Troutier-Thuilliez, A.-L.; Taviot-Guého, C.; Cellier, J.; Hintze-Bruening, H.; Leroux, F. Layered Particle-Based Polymer Composites for Coatings: Part I. Evaluation of Layered Double Hydroxides. *Progress in Organic Coatings* **2009**, *64* (2–3), 182–192. https://doi.org/10.1016/j.porgcoat.2008.09.021.
(61) Meyn, M.; Beneke, K.; Lagaly, G. Anion-Exchange Reactions of Layered Double Hydroxides. *Inorg. Chem.* **1990**, *29* (26), 5201–5207. https://doi.org/10.1021/ic00351a013.
(62) Carvalho, H. W. P.; Pulcinelli, S. H.; Santilli, C. V.; Leroux, F.; Meneau, F.; Briois, V. XAS/WAXS Time-Resolved Phase Speciation of Chlorine LDH Thermal Transformation: Emerging Roles of Isovalent Metal Substitution. *Chem. Mater.* **2013**, *25* (14), 2855–2867. https://doi.org/10.1021/cm401352t.
(63) Kasha, M. EnergyTransferMechanismsand the MolecularExciton Model for MolecularAggregates"2. *Radiation Research* **1963**, *20*, 55–71.
(64) Legentil, P.; Leroux, F.; Mahiou, R.; Therias, S.; Boyer, D.; Reveret, F.; Nauton, L.; Thery, V.; Valleix, R.; Chadeyron, G. Elucidating the Effect of the Spacer and the Luminescence Mechanism of SRB

Hosted in a LDH Interlayer. *Mater. Adv.* **2022**, *3* (2), 1200–1211. https://doi.org/10.1039/D1MA00939G.

(65) Rifani, M.; Yin, Y.-Y.; Elliott, D. S.; Jay, M. J.; Jang, S.-H.; Kelley, M. P.; Bastin, L.; Kahr, B. Solid State Dye Lasers from Stereospecific Host-Guest Interactions. *J. Am. Chem. Soc.* **1995**, *117* (28), 7572–7573. https://doi.org/10.1021/ja00133a042.

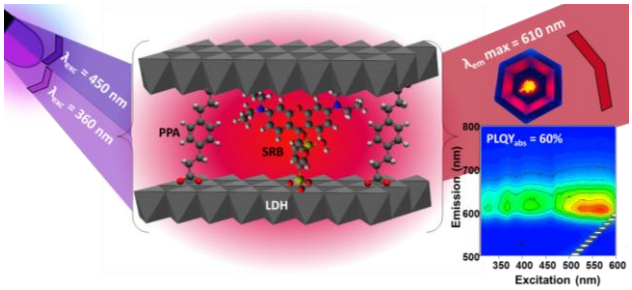

For Table of Contents Only